

1-1-2002

## Search for [Formula presented] and [Formula presented] Oscillations at NuTeV

S. Avvakumov  
*University of Rochester*

T. Adams  
*Kansas State University*

A. Alton  
*Kansas State University*

L. de Barbaro  
*Northwestern University*

P. de Barbaro  
*University of Rochester*

*See next page for additional authors*

Follow this and additional works at: [https://repository.lsu.edu/physics\\_astronomy\\_pubs](https://repository.lsu.edu/physics_astronomy_pubs)

---

### Recommended Citation

Avvakumov, S., Adams, T., Alton, A., de Barbaro, L., de Barbaro, P., Bernstein, R., Bodek, A., Bolton, T., Brau, J., Buchholz, D., Budd, H., Bugel, L., Conrad, J., Drucker, R., Fleming, B., Frey, R., Formaggio, J., Goldman, J., Goncharov, M., Harris, D., Johnson, R., Kim, J., Koutsoliotas, S., Lamm, M., Marsh, W., Mason, D., McDonald, J., McFarland, K., McNulty, C., Naples, D., Nienaber, P., Radescu, V., & Romosan, A. (2002). Search for [Formula presented] and [Formula presented] Oscillations at NuTeV. *Physical Review Letters*, 89 (1) <https://doi.org/10.1103/PhysRevLett.89.011804>

This Article is brought to you for free and open access by the Department of Physics & Astronomy at LSU Scholarly Repository. It has been accepted for inclusion in Faculty Publications by an authorized administrator of LSU Scholarly Repository. For more information, please contact [ir@lsu.edu](mailto:ir@lsu.edu).

---

## Authors

S. Avvakumov, T. Adams, A. Alton, L. de Barbaro, P. de Barbaro, R. H. Bernstein, A. Bodek, T. Bolton, J. Brau, D. Buchholz, H. Budd, L. Bugel, J. Conrad, R. B. Drucker, B. T. Fleming, R. Frey, J. A. Formaggio, J. Goldman, M. Goncharov, D. A. Harris, R. A. Johnson, J. H. Kim, S. Koutsoliotas, M. J. Lamm, W. Marsh, D. Mason, J. McDonald, K. S. McFarland, C. McNulty, D. Naples, P. Nienaber, V. Radescu, and A. Romosan

# A Search for $\nu_\mu \rightarrow \nu_e$ and $\bar{\nu}_\mu \rightarrow \bar{\nu}_e$ Oscillations at NuTeV

S. Avvakumov<sup>8</sup>, T. Adams<sup>4</sup>, A. Alton<sup>4</sup>, L. de Barbaro<sup>5</sup>, P. de Barbaro<sup>8</sup>, R. H. Bernstein<sup>3</sup>, A. Bodek<sup>8</sup>, T. Bolton<sup>4</sup>, J. Brau<sup>6</sup>, D. Buchholz<sup>5</sup>, H. Budd<sup>8</sup>, L. Bugel<sup>3</sup>, J. Conrad<sup>2</sup>, R. B. Drucker<sup>6</sup>, B. T. Fleming<sup>2</sup>, R. Frey<sup>6</sup>, J.A. Formaggio<sup>2</sup>, J. Goldman<sup>4</sup>, M. Goncharov<sup>4</sup>, D. A. Harris<sup>8</sup>, R. A. Johnson<sup>1</sup>, J. H. Kim<sup>2</sup>, S. Koutsoliotas<sup>2</sup>, M. J. Lamm<sup>3</sup>, W. Marsh<sup>3</sup>, D. Mason<sup>6</sup>, J. McDonald<sup>7</sup>, K. S. McFarland<sup>8,3</sup>, C. McNulty<sup>2</sup>, D. Naples<sup>7</sup>, P. Nienaber<sup>3</sup>, V. Radescu<sup>7</sup>, A. Romosan<sup>2</sup>, W. K. Sakumoto<sup>8</sup>, H. Schellman<sup>5</sup>, M. H. Shaevitz<sup>2</sup>, P. Spentzouris<sup>2</sup>, E. G. Stern<sup>2</sup>, N. Suwonjandee<sup>1</sup>, M. Tzanov<sup>7</sup>, M. Vakili<sup>1</sup>, A. Vaitaitis<sup>2</sup>, U. K. Yang<sup>8</sup>, J. Yu<sup>3</sup>, G. P. Zeller<sup>5</sup>, and E. D. Zimmerman<sup>2</sup>

<sup>1</sup>University of Cincinnati, Cincinnati, OH 45221

<sup>2</sup>Columbia University, New York, NY 10027

<sup>3</sup>Fermi National Accelerator Laboratory, Batavia, IL 60510

<sup>4</sup>Kansas State University, Manhattan, KS 66506

<sup>5</sup>Northwestern University, Evanston, IL 60208

<sup>6</sup>University of Oregon, Eugene, OR 97403

<sup>7</sup>University of Pittsburgh, Pittsburgh, PA 15260

<sup>8</sup>University of Rochester, Rochester, NY 14627

(November 19, 2018)

Limits on  $\nu_\mu \rightarrow \nu_e$  and  $\bar{\nu}_\mu \rightarrow \bar{\nu}_e$  oscillations are extracted using the NuTeV detector with sign-selected  $\nu_\mu$  and  $\bar{\nu}_\mu$  beams. In  $\bar{\nu}_\mu$  mode, for the case of  $\sin^2 2\alpha = 1$ ,  $\Delta m^2 > 2.6 \text{ eV}^2$  is excluded, and for  $\Delta m^2 \gg 1000 \text{ eV}^2$ ,  $\sin^2 2\alpha > 1.1 \times 10^{-3}$ . The NuTeV data exclude the high  $\Delta m^2$  end of  $\bar{\nu}_\mu \rightarrow \bar{\nu}_e$  oscillations parameters favored by the LSND experiment without the need to assume that the oscillation parameters for  $\nu$  and  $\bar{\nu}$  are the same. We present the most stringent experimental limits for  $\nu_\mu(\bar{\nu}_\mu) \rightarrow \nu_e(\bar{\nu}_e)$  oscillations in the large  $\Delta m^2$  region.

PACS numbers: 14.60.Pq, 13.15.+g ; UR-1640 to be published in Phys. Rev. Lett.

Experimental evidence for oscillations among the three neutrino generations has been recently reported. For two-generation mixing, the probability that a neutrino created as type  $\nu_1$  oscillates to type  $\nu_2$  is:

$$P(\nu_1 \rightarrow \nu_2) = \sin^2 2\alpha \sin^2 \left( \frac{1.27 \Delta m^2 L}{E_\nu} \right), \quad (1)$$

where  $\Delta m^2$  is the mass squared difference between the mass eigenstates in  $\text{eV}^2$ ,  $\alpha$  is the mixing angle,  $E_\nu$  is the incoming neutrino energy in GeV, and  $L$  is the distance between the points of creation and detection in km.

Data from the Super-Kamiokande atmospheric neutrino experiment [1] have been interpreted as evidence for  $\nu_\mu \rightarrow \nu_\tau$  oscillations with  $\sin^2 2\alpha > 0.88$  and  $1.6 \times 10^{-3} < \Delta m^2 < 4 \times 10^{-3} \text{ eV}^2$ . The LSND experiment has reported [3] a signal consistent with  $\bar{\nu}_\mu \rightarrow \bar{\nu}_e$  oscillations with  $\sin^2 2\alpha \approx 10^{-2}$  and  $\Delta m^2 \gtrsim 1 \text{ eV}^2$ . The solar neutrino experiments, and most recently SNO [2] have reported evidence for oscillations of  $\nu_e \rightarrow (\nu_\mu, \nu_\tau)$  with  $\Delta m^2 < 10^{-3} \text{ eV}^2$ . Within a three-generation mixing scenario and under the assumption that the  $\Delta m^2$  values for  $\nu$  and  $\bar{\nu}$  are the same, it is not possible to simultaneously accommodate the Super-Kamiokande, LSND, and SNO results. Therefore, experimental searches for oscillations with both  $\nu$  and  $\bar{\nu}$  beams are of interest. In this letter, we report on a search for oscillations in both the  $\nu_\mu \rightarrow \nu_e$  and  $\bar{\nu}_\mu \rightarrow \bar{\nu}_e$  channels using a new sign-selected neutrino beam.

High-purity  $\nu$  and  $\bar{\nu}$  beams are provided by the new Sign-Selected Quadrupole Train (SSQT) beamline at the Fermilab Tevatron during the 1996-1997 fixed target run. Hadrons are produced when the 800 GeV primary proton beam interacts in a BeO target located 1436 m upstream of the neutrino detector. Sign-selected secondary particles of specified charge (mean energy of about 250 GeV) are directed in a 221 m beamline towards a 320 m decay region, while oppositely charged (and neutral) mesons are stopped in beam dumps. Two-body decays of the focused pions yield  $\nu_\mu$  ( $\bar{\nu}_\mu$ ) with a mean energy of  $\approx 75$  GeV. Two-body decays of the focused kaons yield  $\nu_\mu$  ( $\bar{\nu}_\mu$ ) with a mean energy of  $\approx 200$  GeV. Muons are stopped in a 915 m steel/earth shield.

The energy and spatial distributions of  $\nu_\mu$  ( $\bar{\nu}_\mu$ ) CC events in the detector provide a determination of the flux of pions and kaons in the decay channel (used in the determination of the predicted  $\nu_e$  and  $\bar{\nu}_e$  fluxes). For  $\nu_\mu$  running mode, the predicted energy spectra for  $\nu_\mu$ ,  $\bar{\nu}_\mu$ , and  $(\nu_e + \bar{\nu}_e)$  CC events are shown in Figure 1(a). The corresponding spectra for  $\bar{\nu}_\mu$  running mode are shown in Figure 1(b). The  $\nu_\mu$  ( $\bar{\nu}_\mu$ ) beam contains a 1.7% (1.6%)  $\nu_e$ 's ( $\bar{\nu}_e$ 's) 93% and 70% of which are produced from  $K^\pm \rightarrow \pi^0 e^\pm \bar{\nu}_e^{(-)}$ , for  $\nu$  and  $\bar{\nu}$  modes, respectively. The proton beam is incident on the production target at an angle such that forward neutral kaons do not point at the detector. This greatly reduces the electron neutrino flux from neutral kaon decays (which is more difficult to

model). The error in the predicted electron neutrino flux is reduced from 4.1% (in CCFR [4]) to 1.4% (NuTeV).

The NuTeV detector [5] is an upgrade of the CCFR detector [6]. It consists of an 18 m long, 690 ton total absorption target-calorimeter with a mean density of  $4.2 \text{ g/cm}^3$ . Muon energy is measured by a 10 m long iron toroidal spectrometer. The target consists of 168 steel plates, each  $3 \text{ m} \times 3 \text{ m} \times 5.15 \text{ cm}$ , instrumented with liquid scintillation counters placed every two steel plates and drift chambers every four plates. The separation between consecutive scintillation counters corresponds to six radiation lengths. The energy resolution of the target calorimeter is  $\Delta E_h/E_h \approx 0.85/\sqrt{E_h}(\text{GeV})$ , and  $\Delta E_e/E_e \approx 0.50/\sqrt{E_e}(\text{GeV})$  for hadrons and electrons, respectively. The muon momentum resolution is  $\Delta p_\mu/p_\mu = 0.11$ . The NuTeV detector is calibrated continuously every accelerator cycle (once a minute) with beams of electrons, muons, and hadrons during the slow spill part of the cycle.

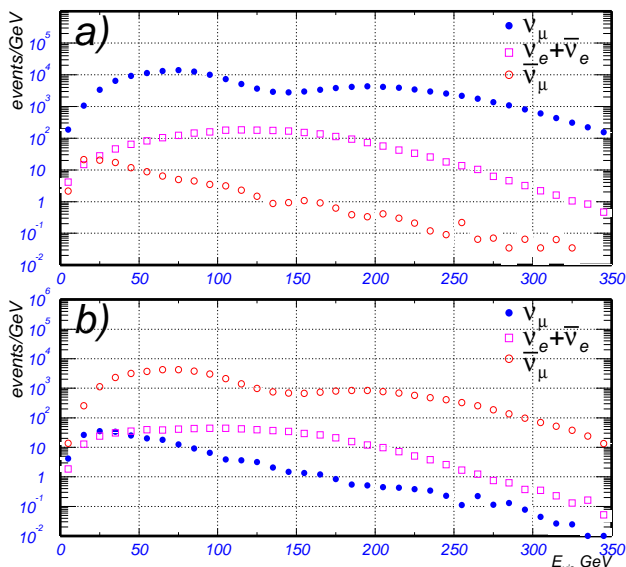


FIG. 1. (a) The predicted visible energy spectra for  $\nu_\mu$ ,  $\bar{\nu}_\mu$ , and  $(\nu_e, \bar{\nu}_e)$  CC-events in  $\nu_\mu$  running mode. (b) The corresponding spectra for  $\bar{\nu}_\mu$  running mode. The predictions come from a beam simulation tuned to agree with the observed number of  $\nu_\mu$  or  $\bar{\nu}_\mu$  CC events in each running mode.

While the neutrinos arrived in gates a few *msec* wide, the calibration beam arrived in a different gate 20 *sec* long, followed by an off-spill cosmic ray gate for background measurement. These continuous test beam calibrations yield a reduction in the hadron energy scale error from 1% (in CCFR [6]) to 0.43% (in NuTeV [5]).

The event sample used in this analysis is similar to that used in the recent precise NuTeV measurement of the electroweak mixing angle [7] with additional fiducial cuts, and  $E_{\text{cal}} > 30 \text{ GeV}$ . The data sample consists of  $1.5 \times 10^6$   $\nu$  events and  $0.35 \times 10^6$   $\bar{\nu}$  events with a mean visible energy in the calorimeter ( $E_{\text{cal}}$ ) of 74 GeV and

56 GeV, respectively. The observed neutrino events are separated into CC and NC candidates. Both CC and NC interactions initiate a cascade of hadrons in the target that is registered in both the scintillation counters and drift chambers. Muon neutrino CC events are distinguished by the presence of a final state muon, which typically penetrates well beyond the hadronic shower and deposits energy in a large number of consecutive scintillation counters. NC events usually have no final state muon and deposit energy over a range of counters typical of a hadronic shower (about ten counters  $\approx 1 \text{ m}$  of steel). For each event, the length ( $L$ ) is defined as the number of scintillation counters between the interaction vertex and the last counter consistent with at least single muon energy deposition. A pure sample of  $\nu_\mu N \rightarrow \mu^- X$   $\nu_\mu$  charged current events is obtained from a ‘long’ sample with  $L \geq 29$  for  $\nu$  running mode ( $L \geq 28$  for  $\bar{\nu}$ ). The ‘short’ event sample consists of events with  $L \leq 28$  for  $\nu$  running mode ( $L \leq 27$  for  $\bar{\nu}$ ). Events with a ‘short’ length are primarily NC induced and originate from:

1.  $\nu_{\mu,e} N \rightarrow \nu_{\mu,e} X$ ;  $\nu_{\mu,e}$  NC events; ( $\approx 65\%$ );
2.  $\nu_\mu N \rightarrow \mu^- X$ ;  $\nu_\mu$  short CC events with muons which range out or exit the side of the calorimeter (25% for  $\nu$ , 15% for  $\bar{\nu}$ );
3.  $\nu_e N \rightarrow e X$   $\nu_e$  CC events (10% for  $\nu$ , 15% for  $\bar{\nu}$ );
4.  $\mu N \rightarrow \mu X$ ; steep cosmic ray interactions (2% for  $\nu$  and 9% for  $\bar{\nu}$ ).

The electron produced in a  $\nu_e$  CC event (source 3) deposits energy in a few counters immediately downstream of the interaction vertex; this changes the longitudinal energy deposition profile of the shower. The energy profile is characterized by the ratio of the sum of the energy deposited in the first three scintillation counters to the total visible energy in the calorimeter  $E_{\text{cal}}$ :

$$\eta_3 \equiv \frac{E_1 + E_2 + E_3}{E_{\text{cal}}}, \quad (2)$$

where  $E_i$  is the energy deposited in the  $i^{\text{th}}$  scintillation counter downstream of the interaction vertex, and  $E_{\text{cal}}$  is the sum of the energy in the 20 scintillation counters downstream (plus 1 upstream) of the vertex. We similarly define  $\eta_2$  to be the ratio of the sum of the energy deposited in the first two scintillation counters to  $E_{\text{cal}}$ .

Although the electromagnetic shower component is typically much shorter than a hadron shower, NC and  $\nu_e$  CC interactions cannot be separated on an event-by-event basis. However, the difference in the shower profiles can be used to perform a statistical extraction of the number of  $\nu_e$  CC events in the ‘short’ sample using the  $\eta_3$  distribution.

We first assume that (for the same final state hadron energy) hadron showers produced in NC and CC interactions are the same. Any difference in the  $\eta_3$  (or  $\eta_2$ )

distributions of ‘long’ and ‘short’ events is attributed to the presence of  $\nu_e$  CC interactions in the ‘short’ sample. To compare directly the ‘long’ and ‘short’ events, a muon track from the data is added to the ‘short’ events to compensate for the absence of a muon in NC events. The fraction  $f$  of  $\nu_\mu$  CC (source 2) events with a low energy muon contained in the ‘short’ sample which now have two muon tracks is estimated from a detailed Monte Carlo of the experiment. A simulated sample of such events is obtained by choosing ‘long’ events with the appropriate energy distribution from the data to which a second short muon track is added in software. The length of the short track and the angular distribution are obtained from a Monte Carlo of  $\nu_\mu$  CC events.

A sample of  $\nu_e$  CC interactions in our detector is simulated by adding a GEANT [10] generated electromagnetic shower of the appropriate electron energy to the calorimetry counter energies in events in the ‘long’ data sample. There is good agreement between the GEANT simulation of electrons and the test beam data. The energy distribution of the electron neutrinos and the fractional energy transfer  $y$  (in each event) are generated using a detailed Monte Carlo simulation of the experiment. The CC cross section model is tuned to agree with the measured CCFR differential cross sections [8] for  $\nu_\mu$  events. Since the hadron showers in the ‘long’ sample already have a muon track, this sample ( $\nu_e$ CC +  $\mu$ ) can be compared directly with the ‘short’ and ‘long’ samples.

The ‘long’ and ‘short’  $\eta_3$  distributions are further corrected by subtracting the contamination due to cosmic ray events. The cosmic ray component (source 4), which is only important for very low energy bins, is well measured using the off-spill cosmic ray data. Additionally, the  $\eta_3$  distribution of short  $\nu_\mu$  CC events (source 2), normalized to the predicted fraction  $f$ , is subtracted from the ‘short’ event sample.

To extract the number of  $\nu_e$  CC events in each  $E_{\text{cal}}$  bin, we fit the corrected shape of the observed  $\eta_3$  distribution for the ‘short’ sample to a combination of  $\nu_\mu$  CC and  $\nu_e$  CC distributions with appropriate muon additions:

$$[\text{short} + \mu] = \alpha [\nu_\mu \text{CC}] + \beta [\nu_e \text{CC} + \mu]. \quad (3)$$

At this point we improve [9] over the previous CCFR analysis [4] by correcting for additional effects. First, the hadron shower in CC events also includes the contribution of photons that are radiated from the muon during the CC scattering process. These photons are not present in hadron showers of NC events. A correction is applied by using the PYTHIA Monte Carlo [11] to generate the spectrum of photons radiated by the muon in CC events. The parameters in PYTHIA that govern the emission of photons are tuned to yield agreement with the radiative corrections formalism of deRujula [12]. Second, the procedures of adding a muon in software to the ‘short’ sample (to model a ‘long’ event) and of modeling

electron neutrino events by adding GEANT-generated electromagnetic showers to hadron showers from ‘long’ events are corrected for imperfect modeling using a full LEPTO/GEANT/GHEISHA simulation of the experiment and analysis procedures. In the GEANT simulation of neutrino events, the Lund Model is used to generate the initial particle composition of hadron showers. The entire experimental procedure is simulated with the beam Monte Carlo ( $\nu_e, \bar{\nu}_e$ ) flux as input. Modeling corrections are extracted for each  $E_{\text{cal}}$  bin from the small difference between the extracted ( $\nu_e, \bar{\nu}_e$ ) flux using simulated data and the flux extracted using perfect modeling in the Monte Carlo.

The absolute flux of  $\nu_e$ ’s is taken as the average of the results from analyses done using the  $\eta_3$  and  $\eta_2$  variables (the statistical error from the  $\eta_3$  analysis is used). An additional systematic error (2.3% in neutrino mode and 0.6% in antineutrino mode) is included to account for this difference. This systematic error for antineutrinos is smaller because the final state positron carries a much larger fraction of the energy in  $\bar{\nu}_e$  CC events.

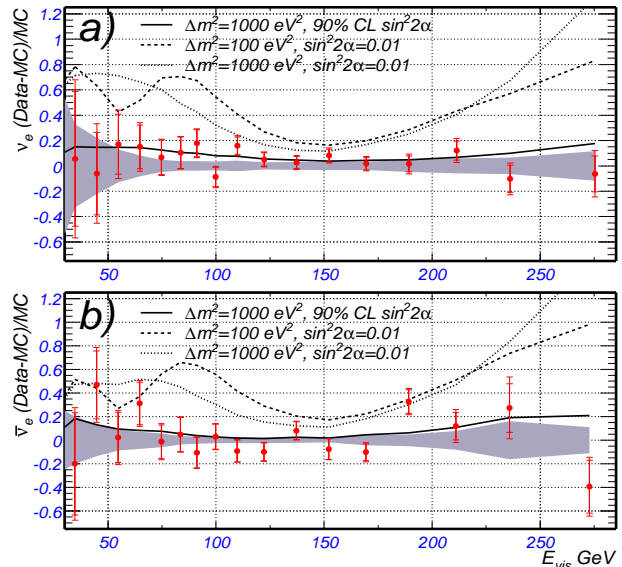


FIG. 2. The ratio of the detected over predicted numbers of ( $\nu_e, \bar{\nu}_e$ ) events versus visible energy minus 1. The curves correspond to the predictions for oscillations with  $\sin^2 2\alpha = 0.01$ , and  $\Delta m^2$  of 100 and 1000  $\text{eV}^2$ . The solid line is the 90% confidence upper limit for  $\Delta m^2 = 1000 \text{eV}^2$ . The shaded area corresponds to the systematic error band.

For the oscillation search we measure the absolute flux of  $\nu_e$ ’s at the detector and compare it to the flux predicted by a detailed beamline simulation [7,9]. In order to extract limits on oscillations, the data are fitted by forming a  $\chi^2$  which incorporates the Monte Carlo generated effect of oscillations and terms with coefficients accounting for systematic uncertainties. A best fit  $\sin^2 2\alpha$  is determined for each  $\Delta m^2$  by minimizing the  $\chi^2$  as a function of  $\sin^2 2\alpha$  and these systematic coefficients. Fig-

ure 2 show the ratios of the measured rate of  $(\nu_e, \bar{\nu}_e)$  CC events to the Monte Carlo predictions minus 1. The inner errors are the statistical errors. In order to show the magnitude of the systematic errors, the outer errors include all systematic errors added in quadrature (in the analysis all correlations are taken into account). The shaded area in the figure corresponds to the systematic error band from uncertainties in the predicted electron flux (primarily from the error in the  $K^\pm$  branching ratio) and uncertainties in the measured flux at the detector (primarily from the  $\eta_3, \eta_2$  difference, and the 2% error in the electron energy scale). The curves correspond to the predictions for oscillations with  $\sin^2 2\alpha = 0.01$ , and  $\Delta m^2$  of 100 and 1000  $\text{eV}^2$ .

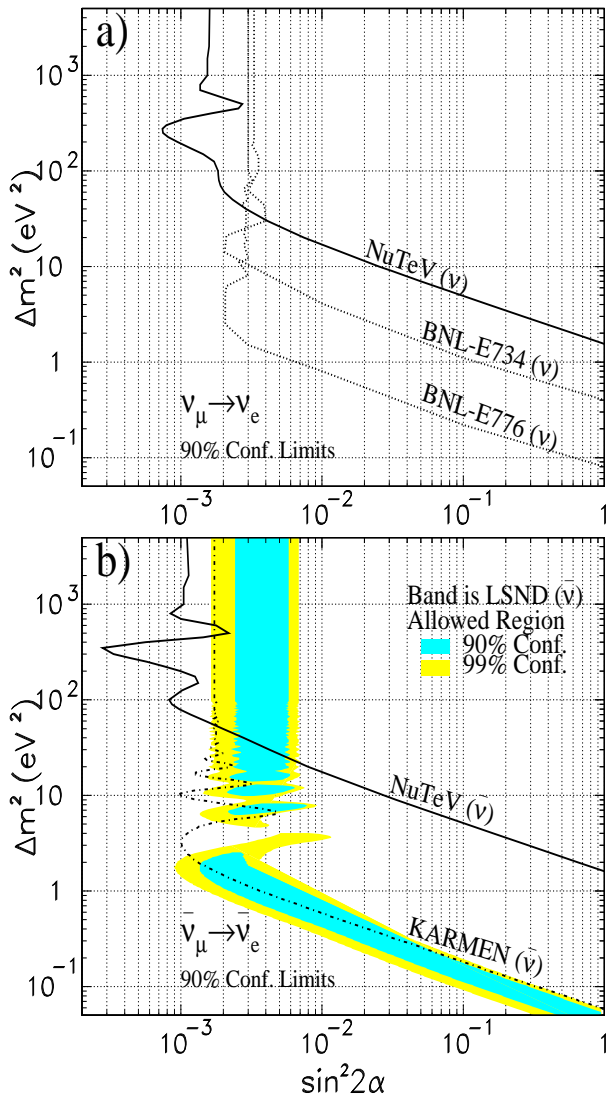


FIG. 3. (a) Excluded region of  $\sin^2 2\alpha$  and  $\Delta m^2$  for  $\nu_\mu \rightarrow \nu_e$  oscillations from the NuTeV analysis at 90% confidence is the area to the right of the dark, solid curve. (b) NuTeV limits for  $\bar{\nu}_\mu \rightarrow \bar{\nu}_e$ .

At all  $\Delta m^2$ , the data are consistent with no observed  $\nu_\mu \rightarrow \nu_e$  oscillations (i.e. the best fit values of  $\sin^2 2\alpha$

are within one standard deviation of zero). The frequentist approach [13] is used to set a 90% confidence upper limit for each  $\Delta m^2$ . The limit in  $\sin^2 2\alpha$  corresponds to a shift of 1.64 units in  $\chi^2$  from the minimum (including all systematic errors). The 90% confidence upper limit is shown in Fig. 3(a) for  $\nu_\mu \rightarrow \nu_e$ . Also shown are limits from BNL-E734 [14] and BNL-E776 [15]. For  $\sin^2 2\alpha = 1$ ,  $\Delta m^2 > 2.4 \text{ eV}^2$  is excluded, and for  $\Delta m^2 \gg 1000 \text{ eV}^2$ ,  $\sin^2 2\alpha > 1.6 \times 10^{-3}$  (the best fit is at 1000  $\text{eV}^2$  is  $\sin^2 2\alpha = (0.4 \pm 0.9 \times 10^{-3})$ ). In the large  $\Delta m^2$  region, NuTeV provides improved limits for  $\nu_\mu \rightarrow \nu_e$  oscillations.

Similarly, the limit for  $\bar{\nu}_\mu \rightarrow \bar{\nu}_e$  is shown Fig. 3(b). Also shown are the LSND [3] results and limits from KARMEN [16]. For the case of  $\sin^2 2\alpha = 1$ ,  $\Delta m^2 > 2.6 \text{ eV}^2$  is excluded, and for  $\Delta m^2 \gg 1000 \text{ eV}^2$ ,  $\sin^2 2\alpha > 1.1 \times 10^{-3}$  (the best fit is at 1000  $\text{eV}^2$  is  $\sin^2 2\alpha = (-0.3 \pm 1.1 \times 10^{-3})$ ). In the  $\bar{\nu}_\mu \rightarrow \bar{\nu}_e$  mode, our results exclude the high  $\Delta m^2$  end of  $\bar{\nu}_\mu \rightarrow \bar{\nu}_e$  oscillations parameters favored by the LSND experiment, without the need to assume that the oscillation parameters for  $\nu$  and  $\bar{\nu}$  are the same. These are the most stringent experimental limits [16] for  $\nu_\mu(\bar{\nu}_\mu) \rightarrow \nu_e(\bar{\nu}_e)$  oscillations in the large  $\Delta m^2$  region.

This work was supported by the U.S. Department of Energy, the National Science Foundation, and the Alfred P. Sloan foundation.

- 
- [1] T. Toshito, hep-ex/0105023; S. Fukuda *et al.*, Phys. Rev. Lett. **85**, 3999 (2000).
  - [2] Q. R. Ahmad *et al.*, Phys. Rev. Lett. **87**, 071301 (2001).
  - [3] A. Aguilar *et al.*, Phys. Rev. **D64**, 112007 (2001); plot for  $\bar{\nu}_\mu \rightarrow \bar{\nu}_e$  provided by Jeff Mills.
  - [4] A. Romosan *et al.*, Phys. Rev. Lett. **78**, 2912 (1997).
  - [5] D. A. Harris, J. Yu, *et al.*, Nucl. Instrum. Methods, **A447**, 377 (2000).
  - [6] W. K. Sakumoto *et al.*, Nucl. Instrum. Methods, **A294**, 179 (1990).
  - [7] G. P. Zeller *et al.*, Phys. Rev. Lett. **88**, 091802 (2002).
  - [8] U. K. Yang *et al.*, Phys. Rev. Lett. **87**, 251802 (2001). U. K. Yang, PhD thesis, Univ. of Rochester, 2001(UR-1583), www.pas.rochester.edu/yigal/bodek/yangthesis.ps.
  - [9] S. Avvakumov, PhD thesis, Univ. of Rochester, 2001. (UR-1641, www.pas.rochester.edu/avva/thesis.ps).
  - [10] GEANT, detector description and simulation tool, CERN Program Library Long Writeup W5013.
  - [11] T. Sjöstrand, Comput. Phys. Commun. **82**, 74 (1994).
  - [12] A. De Rujula *et al.*, Nucl. Phys. **B154**, 394 (1979).
  - [13] Particle Data Group, Phys. Rev. **D54**, 164 (1996).
  - [14] L. A. Ahrens *et al.*, Phys. Rev. **D36**, 702 (1987).
  - [15] L. Borodovsky *et al.*, Phys. Rev. Lett. **68**, 274 (1992).
  - [16] B. Armbruster *et al.* hep-ex/0203021.